Available online at BCREC website: https://bcrec.id

Bulletin of Chemical Reaction Engineering & Catalysis, 16 (3) 2021, 673-685

Research Article

Influence of Operational Parameters on Photocatalytic Degradation of Linuron in Aqueous TiO_2 Pillared Montmorillonite Suspension

D. Hadj Bachir[1], H. Boutoumi[1,*], H. Khalaf[1], P. Eloy[2], J. Schnee[2], E.M. Gaigneaux[2]

[1]Laboratoire de Génie Chimique (LGC), Département de Génie des Procédés, Faculté de Technologie, Université Blida 1, BP 270, 09000 Blida, Algeria.
[2]Université Catholique de Louvain, Institute of Condensed Matter and Nanosciences (IMCN), Place Louis Pasteur 1- L04.01.09, 1348 Louvain-la-Neuve, Belgium.

Received: 31st May 2021; Revised: 16th July 2021; Accepted: 16th July 2021
Available online: 18th July 2021; Published regularly: September 2021

Abstract

TiO_2 pillared clay was prepared by intercalation of titan polyoxocation into interlamelar space of an Algerian montmorillonite and used for the photocatalytic degradation of the linuron herbicide as a target pollutant in aqueous solution. The TiO_2 pillared montmorillonite (Mont-TiO_2) was characterized by X-ray photoelectron spectroscopy (XPS), X-Ray diffraction (XRD), X-Ray fluorescence (XRF), scanning electronic microscopy (SEM), thermogravimetry and differential thermal analysis (TG-DTA), Fourier transformed infra-red (FT-IR), specific area and porosity determinations. This physicochemical characterization pointed to successful TiO_2 pillaring of the clay. The prepared material has porous structure and exhibit a good thermal stability as indicated by its surface area after calcination by microwave. The effects of operating parameters such as catalyst loading, initial pH of the solution and the pollutant concentration on the photocatalytic efficiency and COD removal were evaluated. Under initial pH of the solution around seven, pollutant concentration of 10 mg/L and 2.5 g/L of catalyst at room temperature, the degradation efficiency and COD removal of linuron was best then the other operating conditions. It was observed that operational parameters play a major role in the photocatalytic degradation process.

Keywords: Pillared clay; TiO_2–Montmorillonite; linuron; Photocatalysis; Water purification

How to Cite: D. Hadj Bachir, H. Boutoumi, H. Khalaf, P. Eloy, J. Schnee, E.M. Gaigneaux (2021). Influence of Operational Parameters on Photocatalytic Degradation of Linuron in Aqueous TiO_2 Pillared Montmorillonite Suspension. *Bulletin of Chemical Reaction Engineering & Catalysis*, 16(3), 673-685 (doi:10.9767/bcrec.16.3.11108.673-685)

Permalink/DOI: https://doi.org/10.9767/bcrec.16.3.11108.673-685

1. Introduction

Linuron is one of the most important phenylurea herbicides. It has received particular attention in recent years due to its toxicity, being frequently in the surface and underground waters [1]. It inhibits photosynthesis, and its microbiological degradation is slow; it therefore persists in the environment for many weeks or even months after application [2]. Due to its bio recalcitrant and toxic properties [3], it cannot be directly treated by conventional wastewater treatment; the development of new technologies aimed at the easy degradation of such substances is therefore of practical interest. Among these methods, photocatalytic degradation is highly promising because it can operate at ambient temperature and pressure with low energy photons, does not require expensive catalyst, and utilizes natural sunlight [4].

* Corresponding Author.
Email: ybentoumi@ymail.com (H. Boutoumi);
Telp.: +213 25 43 36

TiO_2 induced photocatalysis has attracted intensive attention as a water and wastewater treatment technology to eliminate toxic and recalcitrant organic compounds over the past decades. Owing to its high photocatalytic activity, excellent physical and chemical stability, low cost, non-corrosive, nontoxicity chemical inertness, its optical properties to UV irradiation, and high availability it is a greatly promising material [5,6]. The detailed mechanism of the TiO_2 mediated photodegradation of organic compounds has been extensively described in the literature [7]. However, this semiconductor cannot be easily removed due to the small size of its particles and remains in suspension once the reaction is complete and therefore costly separation methods are necessary [8]. Besides, during the photocatalytic degradation process, the TiO_2 nanoparticles may undergo aggregation due to the instability of the nanosized particle, which may hamper the light incidence on the active centers and consequently reduce its catalytic activity [9,10].

Numerous articles have been reported to use semiconductor pillars to prepare new combined functional clays. Among them, TiO_2-based clay has attracted growing interest because of their low toxicity, such kind of materials being used as photocatalysts for efficient treatment of wastewaters containing toxic organic compounds. The intercalation of titanium into the interlayer of clays is one of the most promising methods for synthesizing titanium pillared clays as well as improving the photocatalytic activity for the degradation of organic pollutants in water [11–14].

The aim of this work is the synthesis of TiO_2-pillared montmorillonite as a photocatalyst for the degradation of herbicide (linuron) as a recalcitrant pollutant through the coupling of adsorption and photocatalysis in addition to its recovery by filtration for its contrast to nanoscale TiO_2. The photocatalytic performance of the prepared material and the effect of some operational parameters on the degradation rate, such as the amount of catalyst, the pH of the medium and the concentration of the pollutant are examined.

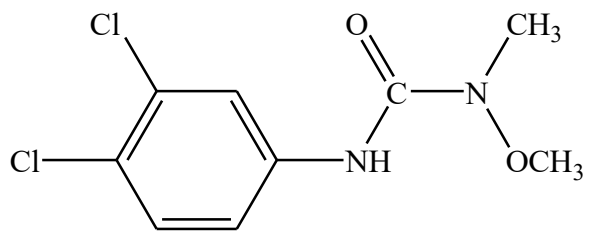

Figure 1. Chemical structure of Linuron.

2. Materials and Methods

2.1 Material and Reagents

The starting clay was a bentonite obtained from the Roussel deposit of Maghnia (Algeria). It is reported to be composed essentially of montmorillonite with minor impurities (quartz, feldspar, calcite). The structural formula is $Na_{0.35}K_{0.01}Ca_{0.02}(Si_{3.89}Al_{0.11})(Al_{1.60}Mg_{0.32}Fe_{0.08})O_{10}(OH)_2$. The cation exchange capacity (CEC) of the montmorillonite is 90 meq per 100 g of bentonite, its chemical composition (wt%) is: SiO_2 69.4; Al_2O_3 14.7; Fe_2O_3 1.2; MgO 1.1; CaO 0.3; Na_2O 0.5; K_2O 0.8; TiO_2 0.2, and its mass loss by ignition at 1173 K is 11%.

This bentonite was purified using a sedimentation process to obtain a purified bentonite with high montmorillonite content. The pure bentonite was then modified through cation exchange with a NaCl (1 M) aqueous solution to obtain Mont-Na [15]. HCl was purchased from Fluka and Titanium (IV) isopropoxide [$Ti(OC_3H_7)_4$] (100%) from Prolabo. The pollutant used in this study is a phenyl urea herbicide (Linuron) precisely 3-(3,4-dichlorophenyl)-1-methoxy-methylurea (99.9%), it is from Sigma. All aqueous solutions were prepared with deionized water. The chemical structure of the Linuron is shown in Figure 1.

2.2 Preparation of the Photocatalyst

2.2.1 Synthesis of TiO_2 pillared montmorillonite (Mont-TiO_2)

The TiO_2 pillared clays were prepared as reported by the literature [16]. The titanium polycation was prepared in a chlorhydric acid (HCl, 1 M) aqueous solution by addition of titanium isopropoxide drop by drop. The molar ratio HCl/Ti was 4. The obtained solution was then dropped slowly into the swelled clay with molar ratio Ti/clay=10 mmol/g [15,16]. The reaction temperature was maintained at 50 °C with a continuous mechanical agitation for 3 h; the obtained solid suspension was stirred for 15 additional hours. This suspension was then centrifuged and washed several times with distilled water to remove excessive HCl, dried at 40 °C during 72 h. Finally, the modified clay was calcined during 15min in a microwave apparatus at 800 W. Then the solid pillared clay sample was grounded in powder and named Mont-TiO_2.

2.2.2 Characterization

X-ray diffraction (XRD) patterns of the resulting materials were performed on a PANa-

lytical: XPERT-PRO diffractometer using Cu-Kα source operated at 45 kV and 40 mA. The samples were measured at room temperature in the range from 2θ = 3° to 90°. XPS analyses were performed on a Kratos Axis Ultra spectrometer (Kratos Analytical–Manchester–UK) equipped with a monochromatised aluminium X-ray source (powered at 10 mA and 15 kV). Elemental analysis of the samples was carried out on an X-ray fluorescence spectrometer FRX 303 Siemens. Fourier transformed infra-red (FT-IR) spectra were recorded in the range of 4000 to 400 cm^{-1} on a FT-IR BRUKER, TENSOR 27 spectrophotometer. Scanning electron microscopy (SEM) PHILIPS ESEM XL 30 with a tungsten filament was used to examine the morphology of the investigated samples using conductive carbon paint. Nitrogen adsorption-desorption isotherms of the prepared materials were obtained at 77 K by Micromeritics Tristar 3000. BET surface area and total pore volume were calculated from the adsorption isotherm. Thermogravimetry and Differential thermal analysis (TG-DTA) were performed on a Simultaneous Thermal Analyzer STA 409 PC LUXX from NETZSCH on masses of approximately 40 mg of the different prepared clay samples at a heat rate of 10 °C/min from room temperature to a maximum temperature of 900 °C under air.

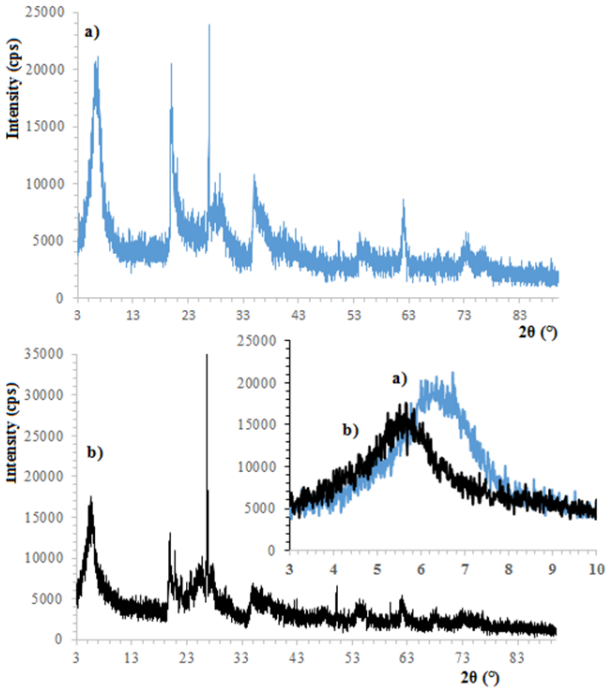

Figure 2. XRD pattern of a) Mont-Na and b) Mont-TiO_2.

2.3 Preparation of Initial Synthetic Wastewater

The linuron herbicide was used as target compound in the experiments. The initial solution was 10 mg/L of this herbicide dissolved in purified water, protected from light and left for one night in order to reach total solubilization.

2.3.1 Direct photolysis of Linuron

Before starting the photocatalytic reactions, photolysis of the herbicide was carried out by putting 80 mL of the polluted solution of 10 mg/L at pH = 6.7 under UV radiation in the absence of catalyst; the degradation kinetics was followed for 3 h with a sample taken every every 15 min for 1 h then after every 30 min.

2.3.2 Photocatalysis of linuron

Photocatalytic degradation tests of the herbicide were carried out in a photoreactor using UV lamp (Philips HPK brand lamp) with a 125 W power, the theoretical energy of the lamp being 47W/m^2. 80 mL of the polluted solution of 10 mg/L at pH = 6.7 was used. Prior to photodegradation, the suspension of the photoreactor containing appropriate amount (2.5 g/L) of pillared clay was stirred in the dark for 30 min to establish the adsorption/desorption equilibrium between the photocatalyst and herbicide to be degraded. During the photodegradation experiment, 2 mL aliquots of suspension were collected at regular time intervals, filtered through a 0.45 mm Millipore and analyzed by UV-Vis spectrophotometer in order to determine the concentration of the degraded pollutant.

3. Results and Discussion

3.1 Characterization of the Photocatalyst

3.1.1 X-ray diffraction (XRD) and elemental analysis (XRF)

The X-ray Diffraction patterns of the initial clay (Mont-Na) and the pillared sample (Mont-TiO_2) are shown in Figure 2. The ordered pillaring of layered materials results in the shift of the (001) to lower 2θ region [15,16]. Before intercalation, the typical diffraction peak of Mont-Na at 6.4° corresponds to a basal spacing of 13.81 Å. After intercalation of the titanium polyoxocation and microwave calcination for 15 min, this peak moves to a low angle at 5.5°, which corresponds to a basal spacing of 16.07 Å pointing to an enlargement of the basal spacing of the clay layers by polycations, indicating a successful pillaring process. The characteris-

tic diffraction peak corresponding to (101) reticular plane of anatase form was detected at 25.37° (2θ). Other anatase diffraction peaks appeared at 37.97°, 47.67°, 54.86°, 62.77°, and 75.62° (2θ) [17-18].

X-ray fluorescence was used to determine metal oxide contents in the samples. SiO_2 and TiO_2 were the main components of the modified clay. Na_2O content in the purified montmorillonite was the higher, which suggests that the homogeneous mineral was sodium montmorillonite. For sodic montmorillonite, a lower TiO_2 content (0.07%) was detected. A drastic reduction in the amount of Silicon, Aluminum, Iron and Sodium elements occurs on pillaring with titanium. The major information, resulting from the chemical composition of the investigated samples (Table 1), is the increase of TiO_2 content at the detriment of SiO_2, Al_2O_3 and Na_2O content, which indicates the incorporation of Ti polycations between the silicate layers upon pillaring. The synthesis temperature was 50 °C because it is known that the temperature of the complex solution improves the hydrolysis and polymerization degree of the titanium [19]. The amount of TiO_2 increases to 36.5%, this increase in titanium content with corresponding decrease in the amount of exchangeable cations points to replacement of interlamellar cations with stable titanium oxide pillars, this is proportional to the development of microporosity in the clay and to the extent of thermal stability. This clay is therefore expected to have more pillars and a bigger degree of lamellar ordering and stability [20].

3.1.2 XPS analysis of Mont-Na and Mont-TiO_2

The binding energy (BE) and composition in the 10 nm depth of Mont-Na and Mont-TiO_2 determined from XPS experiments are presented in Table 2. In TiO_2 pillared montmorillonite the presence of expected elements (Ti, Al, Si, and O) is observed. A small amount of Fluor (0.4 at. %) which is an impurity that may come during the formation of sodium montmorillonite is also noted [21]. The two peaks (Figure

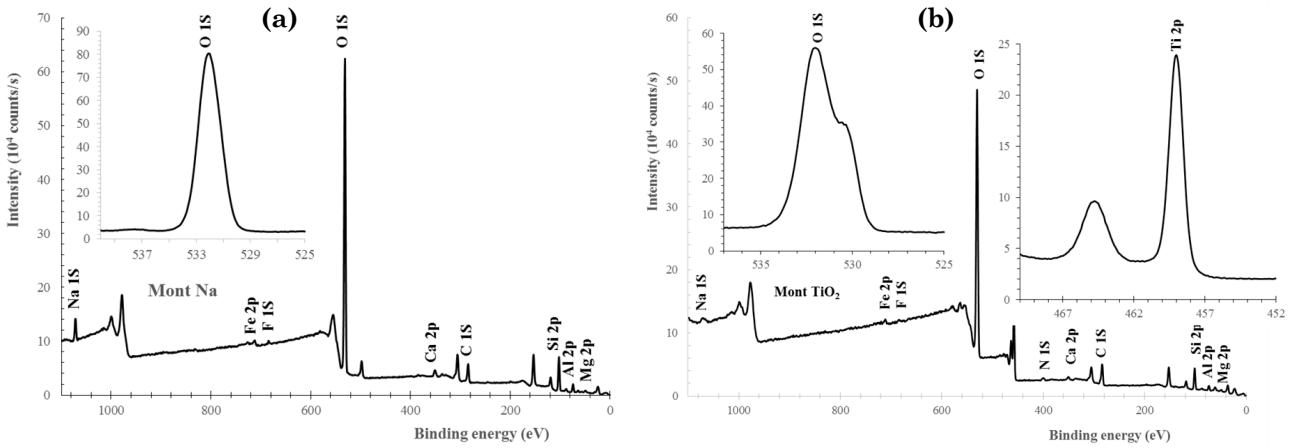

Figure 3. (a) Mont-Na XPS spectrum with enlargement of O1s region and (b) Mont-TiO_2 XPS spectrum with Ti2p and O1s enlargement regions.

Table 1. Elemental analysis of the Mont-Na and Mont-TiO_2.

Samples/oxides (%)	SiO_2	Al_2O_3	Fe_2O_3	CaO	MgO	Na_2O	K_2O	TiO_2
Mont-Na	52.64	21.17	2.30	0.43	1.89	1.93	0.74	0.07
Mont-TiO_2	31.78	9.50	1.12	0.58	1.75	0.13	0.80	36.51

Table 2. Binding energies (BEs, eV), atomic percentage and atomic ratios obtained from XPS experiments performed on Mont-Na and Mont-TiO_2.

Sample	Ti 2p3/2		Si 2p		Al 2p		C 1s		Ti/Si	Al/Si
	BE	At%	BE	At%	BE	At%	BE	At%		
Mont-Na	-	uld*	103	20.1	74.9	7.8	284.8	9.1	-	0.4
Mont-TiO_2	459.0	6.9	102.9	13.8	74.9	5.5	284.8	13.5	0.5	0.4

uld*: Under the limit detection (0.1%)

3(b)), which binding energy are 459 eV and 464.8 eV, which are attributed to Ti2p3/2 and Ti2p1/2, respectively. Thus, the Ti 2p spectrum of TiO_2-pillared clay catalyst is dominated by species in the Ti^{4+} oxidation state [22]. Binding energy (BE) of Ti 2p3/2 observed at near 459 eV corresponds to bulk TiO_2 [23]. This value is almost the same as the binding energy of 2p3/2 of Ti on TiO_2 [24]. The O1s XPS peak in homogeneous sample (Mont-Na) and TiO_2-pillared montmorillonite (Mont-TiO_2) are represented in Figure 3 (a and b, respectively).

According to the literature [25], the O1s binding energy of Mont-Na was observed at 532.1 eV, and is attributed to the lattice oxygen of the aluminosilicate of montmorillonite [26-27]. In the case of Mont-TiO_2, the O1s peak present a supplementary contribution around 530.2 eV that can be assigned to anatase lattice oxygen [27].

3.1.3 FT-IR spectroscopy

The FT-IR spectra of the sodic montmorillonite (Mont-Na) and the TiO_2-pillared montmorillonite (Mont-TiO_2) are given in Figure 4. The band observed at 3631 cm^{-1} for the sodic clay corresponds to the stretching vibration of the hydroxyl group in Al–OH and Si–OH species and the interlayer water molecules [28]. The introduction of titanium in the sodic montmorillonite by the pillaring process led to broader bands due to the presence of additional new types of –OH groups which is interpreted as an effect of pillaring [13]. Besides, the OH bending peak corresponding to the bound water is detected at 1641 and 1652 cm^{-1} for the prepared material and the one at around 1030 cm^{-1} is attributed to the asymmetric stretching vibration of SiO_2 in tetrahedral form [21,29]. The band in the range of 500 and 1000 cm^{-1} corresponds to the Ti–O stretching vibration of TiO_2 phase; it is attributed to the vibration of Si–O–Ti in the modified montmorillonite [30,31], this suggesting that anatase clusters are strongly bonded to the silicate through a chemical bond [20]. The band corresponds to the Ti–O stretching vibration of TiO_2 phase appear between 500 and 1000 cm^{-1} is attributed to the vibration of Si–O–Ti in Mont-TiO_2 indicating the introduction of TiO_2 between the layer clay.

3.1.4 Nitrogen adsorption–desorption isotherms

The Figure 5 shows the adsorption–desorption isotherms of nitrogen on the Mont-Na and the TiO_2-pillared sample (Mont-TiO_2). The adsorption isotherm of the sodic clay was type II, which could be characteristic of macro

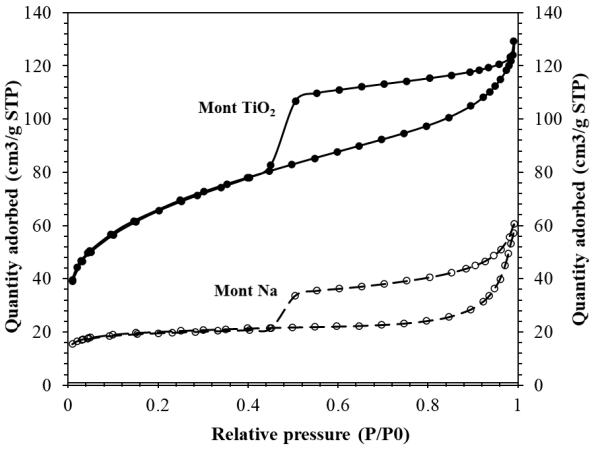

Figure 5. Nitrogen adsorption–desorption isotherms on Mont-Na and Mont-TiO_2 samples.

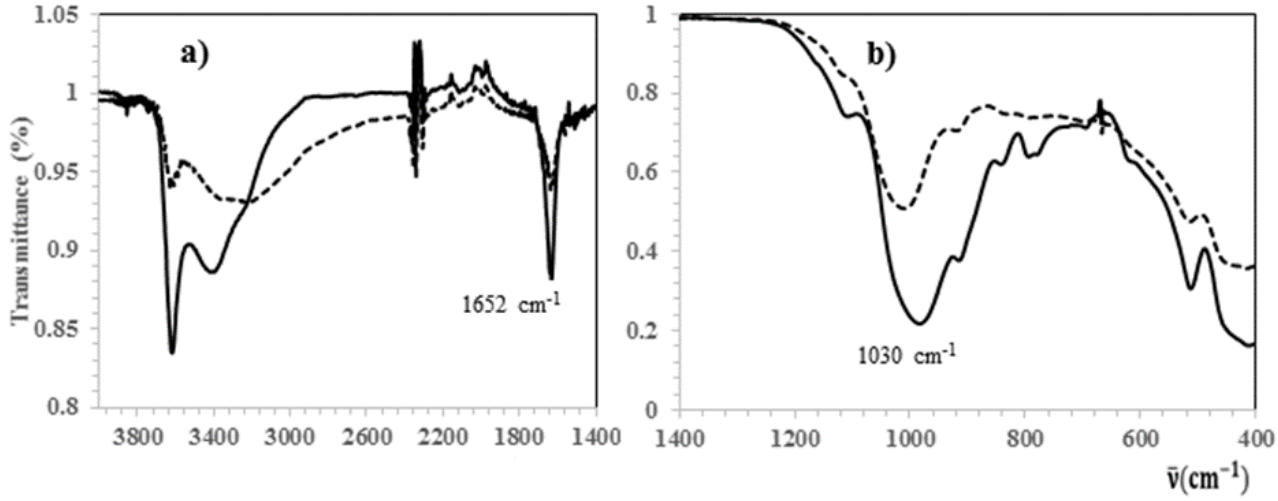

Figure 4. FT-IR spectra of Mont-Na (---) and Mont-TiO_2 (—), (a) 4000-1400 cm^{-1} and (b) 1400-400 cm^{-1}.

or non-porous solids. However the adsorption-desorption isotherms formed a hysteresis loop of the H3 type, which clearly indicates the presence of slit-like pores according to IUPAC classification [32]. The verticality of the drop in the desorption curve at about 0.5 P/P_o suggests that the size of the slit pores are uniform.

The isotherms of the TiO_2 pillared sample seem to be a mixture of type I and II for the adsorption and of type I and IV for the desorption characteristic of solids that include both micropores and mesopores according to [33,34]. Furthermore, the shape of the hysteresis loop for this isotherm is also of type H3 [35], indicating the presence of long slit-shaped and plane-parallel pores in the obtained pillared material. In addition, the desorption branch of the isotherm shows an inflection at about 0.45–0.5 P/P°, typical for many types of layered materials while using nitrogen as an adsorbent [18,21].

The incorporation of TiO_2 pillars between the clay layers considerably increases the surface area; the BET surface area and the total volume of pillared montmorillonite sample (Mont-TiO_2) are indeed much bigger (224 m^2/g and 0.18 cm^3/g) than that of the pristine montmorillonite (62 m^2/g and 0.082 cm^3/g), suggesting the pillaring process leads to a dramatic increase in porosity of layer clays of the prepared material.

3.1.5 ATD/ATG analysis

Thermogravimetric (TG) and differential thermal analysis (DTA) curves of the investigated samples are shown in Figure 6. Thermograms of all samples show an initial endothermic peak within 25 to 130 °C indicating the loss of physisorbed water, this endothermic effect is accompanied by a mass loss of about 9% and 14%, for Mont-Na and Mont-TiO_2 respectively. The weight loss above 200 °C in sodium montmorillonite results from the removal of water initially present between the layers. This collapse slowly continued up to 800 °C.

The gradual weight loss to about 500 °C observed for the pillared clay (Mont-TiO_2) is attributed to the dehydroxylation of OH groups associated with the interlayer polycations due to the pillaring process, between this temperature and 800 °C, a small step loss occurred due to the dehydroxylation of the clay structure [21]. ATD/ATG allows the highlighting of the pillaring process by the dehydroxylation of OH groups associated with the interlayer TiO_2 polycations.

3.1.6 SEM images of the purified and pillared montmorillonite

Figure 7 shows the SEM images of Mont-Na and Mont-TiO_2. These images reveal the variations in morphologies and important structural details. The Mont-Na micrograph shows large particle aggregates with smooth surfaces. This microstructure of the clay was retained in the Mont-TiO_2 after microwave calcination; the same observations have been made by other authors [28,36]. The scanning electron microscopy reveals the structural change of the surface and the increase in porosity.

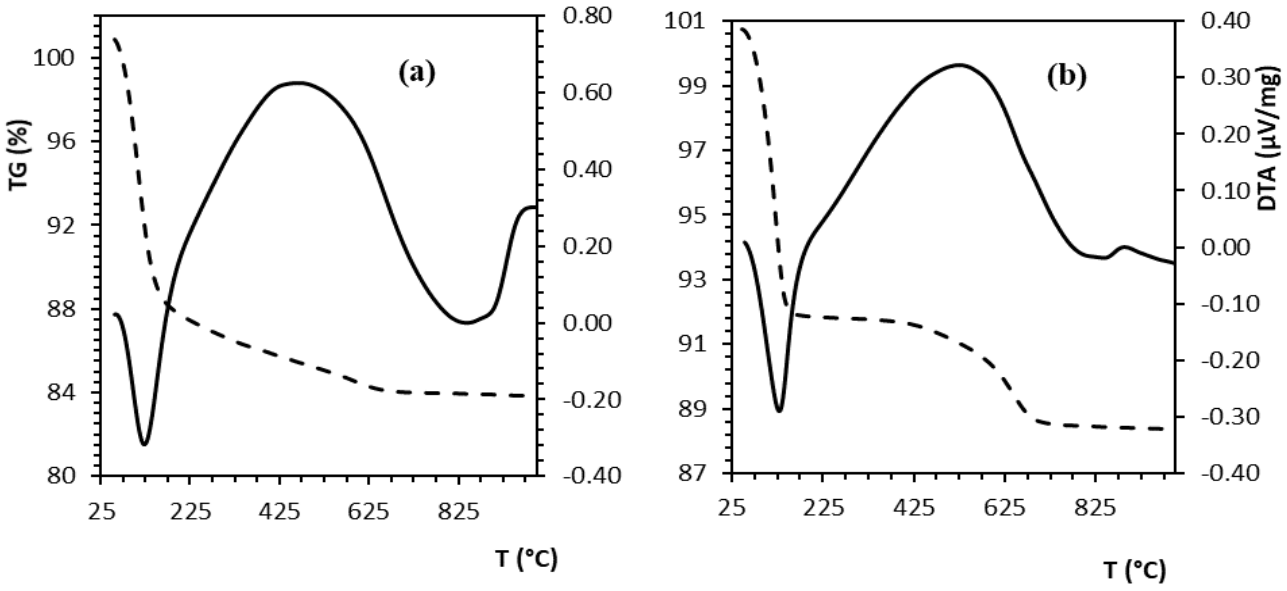

Figure 6. TG/DTA of (a). Mont-Na and (b) Mont-TiO_2 samples.

3.2 Photocatalytic Activity

To test the photocatalytic efficiency of the prepared material, photocatalytic degradation of linuron was carried out under UV irradiation.

3.2.1 Effect of operating parameters

The photocatalyst loading, initial concentration of the pollutant and pH of the solution are among the major factors which influences the efficiency of degradation of pesticides [37]. For this reason the experiments were carried out to find optimum pH value, catalyst loading of the reaction mixture and the initial concentration for the degradation of linuron.

3.2.1.1 Effect of photocatalyst loading

The effect of the catalyst amount was evaluated by means of a change in its load from 1.25 to 5 g/L in the herbicide solution containing 10 mg/L of Linuron at pH 6.7. Figure 8 shows the degradation efficiency measured as a function of the TiO_2 pillared clay catalyst load (Mont-TiO_2). In the absence of the catalyst, no significant decrease in the concentration of Linuron was observed under UV irradiation for about three hours. As can be observed in Figure 8, the removal efficiency of Linuron increases with increasing Mont-TiO_2 dosage, the best photocatalytic activity was obtained for a catalyst concentration of 2.5 g/L.

The increase in the degradation efficiency in the presence of an increased amount of catalyst in the solution is obviously due to the increase of the active material, and thus active sites, resulting in an enhanced free hydroxyl radicals. Hence, further addition of catalyst does not lead to the enhancement of the degradation rate and it remains constant this is probably due to the turbidity of solution reducing the light transmission through the solution [37].

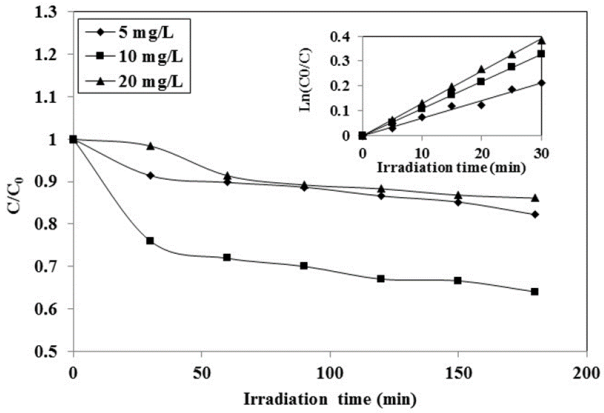

Figure 8. Effect of the amount of Mont-TiO_2 catalyst on the photocatalytic degradation of Linuron. The reaction medium has a pH value of 6.7.

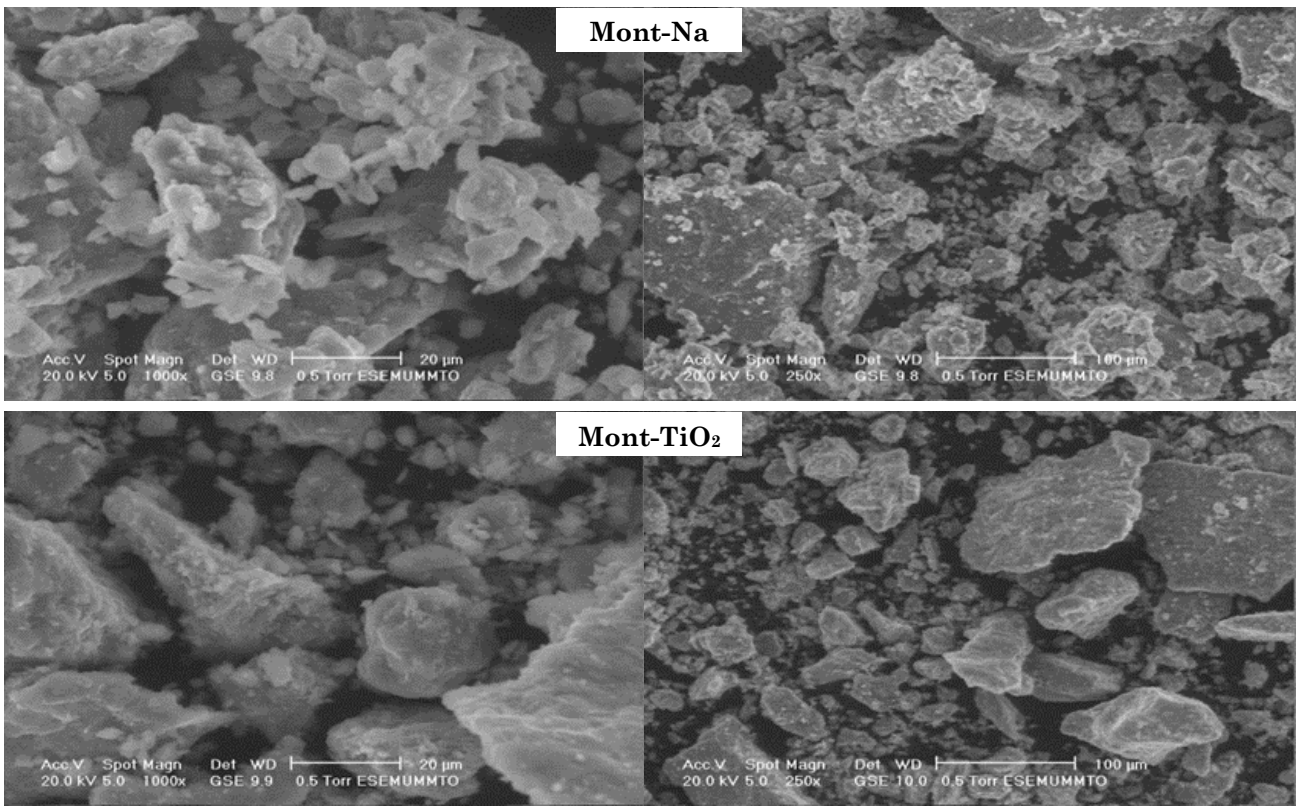

Figure 7. SEM images of Mont- Na and Mont-TiO_2.

3.2.1.2 Effect of initial pH of the reaction medium

The pH of the solution can play a key role in the adsorption and photocatalytic oxidation of pollutants because the electrostatic interaction between semiconductor surface, solvent molecules, substrate and charged radicals formed during photocatalytic oxidation is strongly affected by the pH of the solution. The ionization state of the surface of the photocatalyst can also be protonated and deprotonated under acidic and alkaline conditions respectively as shown in the following reaction [38,39]:

$pH < Pzc \quad Ti{-}OH + H^+ \rightarrow TiOH_2^+$

$pH > Pzc \quad TiOH + OH^- \rightarrow TiO^- + H_2O$

Figure 9 shows the effect of pH on the degradation of Linuron during the photocatalytic process. When HCl is used, in acid watercourses, Linuron is resistant to hydrolysis and becomes more persistent in the environment. This decrease can be explained by the low OH^- concentration which hinders the formation of OH° and subsequently reduces the degradation rate and an inhibition of photocatalytic reactions with chloride ions which adsorb on the surface of TiO_2 and compete with Linuron on the adsorption sites. This inhibition increases with Cl^- concentration particularly at low pH values. In neutral media Linuron is easily hydrolyzed, the inhibition of Cl^- is small hence the maximum number of Linuron molecules are adsorbed on the Mont-TiO_2 surface and consequently result in enhanced photodegradation [40,41]. In an alkaline medium, Linuron degradation decreases due to coulombic repulsion between the negatively charged surface of photocatalyst and hydroxide anions. This fact could prevent the formation of hydroxyl radicals which would result into a decrease in rate of photocatalytic degradation of Linuron [37].

3.2.1.3 Effect of initial linuron concentration

The pollutant concentration is one of the important parameters in photocatalysis processes. Therefore, the effect of herbicide concentration on the degradation efficiency was investigated at different concentrations of Linuron and presented in Figure 10. At low concentration the number of catalytic sites will not be a limiting factor, and the rate of degradation is proportional to the substrate concentration [37]. However, the degradation rate increases with the increase in substrate concentration from 5 to 10 mg/L for Linuron and a further increase in the concentration of substrate led to decrease in the degradation rate in the presence of Mont-TiO_2 photocatalyst because when the concentration of the pollutant increases, more molecules of the compound get adsorbed on the surface of the photocatalyst, the catalyst surface become insufficient, because the amount of catalyst is constant. And photoproducts of linuron can compete with linuron on the surface of TiO_2 pillared montmorillonite leading to surface blocking and finally causing decrease in photoactivity (reduced ability to generate •OH and O_2^- radicals). Consequently, the degradation efficiency of Linuron decreases as the concentration increases [42,43].

3.2.2 Influence of the operating parameters on the efficiency of mineralization in terms of COD by heterogeneous photocatalysis process

Chemical oxygen demand, or COD, is one of the parameters of water quality. It represents the quantity of oxygen necessary to oxidize all the organic matter contained in water. This

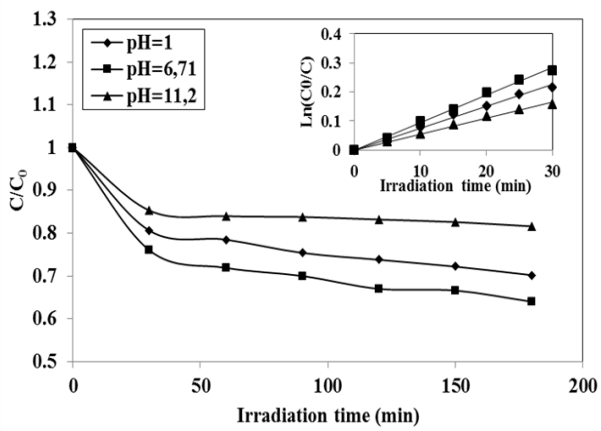

Figure 9. Effect of initial pH on the photocatalytic degradation of linuron.

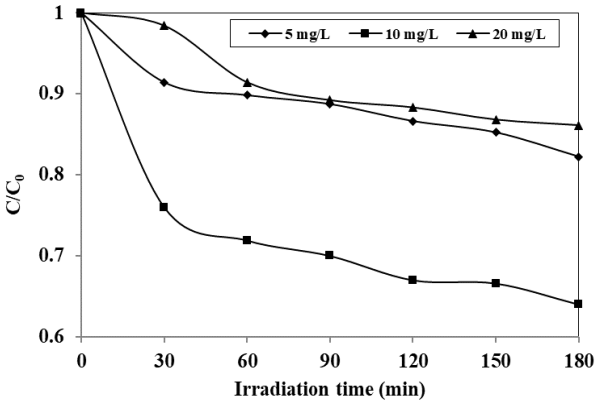

Figure 10. Influence of substrate concentration on the photocatalytic degradation of Linuron in the presence of Mont-TiO_2 photocatalyst.

value is obtained by reacting water samples with a strong oxidant (potassium dichromate) and is expressed in milligrams of oxygen per liter of water. *Chlorophenylurea herbicide* mineralization studies have shown that COD decreases steadily with the degradation kinetics, when one of the operating parameters (photocatalyst loading, initial Linuron concentration or initial pH solution) vary.

3.2.2.1 Effect of photocatalyst dose

Figure 11 depicts COD removal efficiency from the aqueous solution herbicide as a function of photocatalyst dosage. The photocatalyst loading was varied between (1.25 and 5 g/L), the other operational factors (pH, initial concentration) were 6.7 and 10 mg/L, respectively. The results obtained show that the increase in the concentration of the catalyst leads to a decrease in the mineralization of the organic matter. The treatment by heterogeneous photocatalysis of Linuron made it possible to eliminate

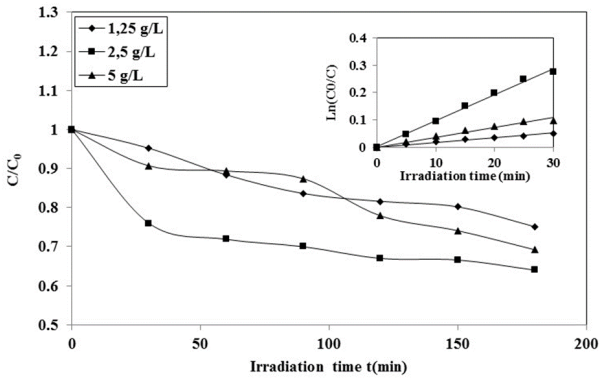

Figure 11. Mineralization kinetics of Linuron (C_0 = 10 mg/L) in term of COD as a function of the photocatalyst loading at pH = 6.7 by heterogeneous photocatalysis.

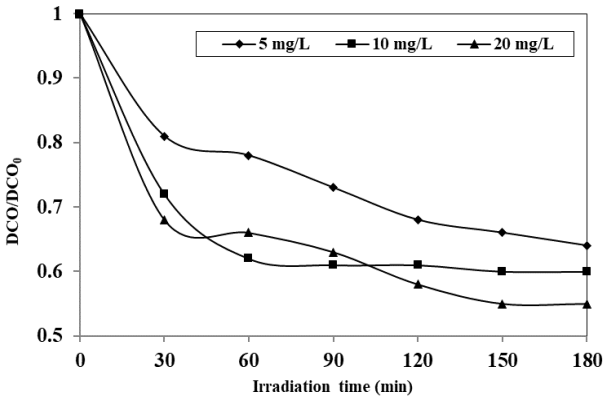

Figure 12. Evolution of the mineralization in terms of COD of an aqueous solution of Linuron according to its concentration, m_{cat} = 2.5 g/L, pH = 6.7.

60% of the organic matter in terms of COD, in approximately 60 min. The optimum adsorbent dose for COD removal was about 2.5 g/mL. It was because of saturation of adsorbent sites and hence the ratios of the initial number of adsorbate molecules to the available adsorption sites of the adsorbent diminished accordingly [44,45].

3.2.2.2 Effect of the initial linuron concentration

The effect of the concentration of the aqueous solution on the COD reduction by the presence of the photocatalyst was studied at various initial concentrations, as shown in Figure 12, other operational factors (pH and adsorbent dosage) were 6.7 and 2.5 g/L, respectively. It can be observed that the mineralization of the herbicide in term of COD decreases with increasing concentration of Linuron because the photonic efficiency diminishes and the photocatalyst surface becomes saturated, whereas photocatalytic processes offer maximum efficiency only when optimum initial concentrations are utilized [46].

3.2.2.3. Effect of initial pH solution

Buffered Linuron solutions (pH = 1 to 9) were irradiated. The initial concentration of herbicide was 10 mg/L and the adsorbent dosage 2.5 g/L. The pH of the aqueous solution plays a decisive role in affecting COD elimination. The results (Figure 13) indicate that at lower pH levels, the removal sharply decreased because of the repulsion between the positively charged functional groups of organic molecules and the positively charged surface of the photocatalyst, the elimination of the herbicide in

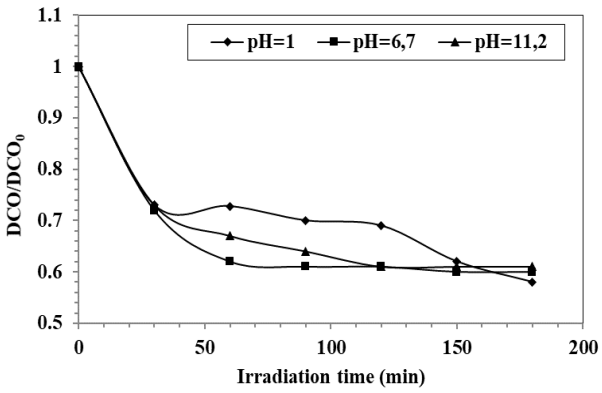

Figure 13. Evolution of the mineralization in terms of COD of an aqueous solution of Linuron according to the pH medium, m_{cat} = 2.5 g/L, $m_{Linuron}$ = 10 mg/L.

term of COD improves with increasing pH because the Linuron molecules bind through electrostatic attraction to the surface of the photocatalyst [47].

4. Conclusion

There are numerous examples of applications of photocatalysts for water treatment, but there is no information about photodegradation in TiO_2 pillared montmorillonite suspensions, of the Linuron which represents one of the most important phenyl-urea herbicides. In this study, TiO_2 pillared clay was synthesized and characterized by DRX, DRF, XPS, FT-IR, ATD/ATG, SEM and BET analysis. The photocatalytic activity of the prepared material was investigated for the photodegradation of the phenylurea herbicide (Linuron) in aqueous solution under UV irradiation. Heterogeneous photocatalyst was successfully synthesized by intercalating TiO_2 pillars into the montmorillonite layers via ion-exchange reaction and subsequent microwave calcination for 10 min. Introduction of TiO_2 between layers clay significantly increase the porosity and surface area of the composite. This product exhibited a good thermal stability as. The prepared TiO_2 pillared clay was highly porous and exhibited a specific surface area of 224 m^2/g and a large pore volume of 0.18 cm^3/g, which was significantly higher as compared to those of the pristine montmorillonite (62 m^2/g and 0.082 cm^3/g). The prepared material is attractive as adsorbent, catalyst, or catalyst support due to its high specific surface area, justifying its potential as support in the heterogeneous photocatalysis. The removal of Linuron and the reduction of COD from aqueous solution using TiO_2 pillared montmorillonite has been experimentally determined and various operating parameters such as, photocatalyst dosage, pH of the reaction medium, and the initial concentration of the effluent on its degradation and COD removal efficiency were investigated. The results show that this photocatalyst is capable of COD removal from aqueous solution and operating parameters can influence the photocatalytic degradation rate of the Linuron herbicide.

Acknowledgment

This work was carried with the support of the Direction Générale de la Recherche Scientifique et du Développement Technologique (*DGRSDT*)/Ministère de l'Enseignement Supérieur et de la recherche Scientifique d'Algérie (MESRS).

Declaration of Interests

The authors declare that they have no known competing financial interests or personal relationships that could have appeared to influence the work reported in this paper.

References

[1] Sánchez-Martin, M.J., Rodriguez-Cruz, M.S., Sánchez-Camazano, M. (2003). Study of the desorption of linuron from soils to water enhanced by the addition of an anionic surfactant to soil-water system. *Water Research*, 37, 3110–3117. DOI: 10.1016/S0043-1354(03)00155-6

[2] Swarcewicz, M., Gregorczyk, A., Sobczak, J. (2013). Comparison of linuron degradation in the presence of pesticide mixtures in soil under laboratory conditions. *Environmental Monitoring and Assessment,* 185, 8109–8114. DOI: 10.1007/s10661-013-3158-7.

[3] Farre´, M.J., Domenech, X., Peral, J. (2006). Assessment of photo-Fenton and biological treatment coupling for Diuron and Linuron removal from water. *Water Research*, 40, 2533–2540. DOI: 10.1016/j.watres.2006.04.034

[4] Katsumata, H., Kobayashi, T., Kaneco, S., Suzuki, T., Ohta, K. (2011). Degradation of linuron by ultrasound combined with photo-Fenton treatment. *Chemical Engineering Journal*, 166, 468–473. DOI: 10.1016/j.cej.2010.10.073

[5] Damardji, B., Khalaf, H., Duclaux, L., David, B. (2009). Preparation of TiO_2-pillared montmorillonite as photocatalyst. Part I. Microwave calcination, characterisation, and adsorption of a textile azo dye. *Applied Clay Science*, 44, 201–205. DOI: 10.1016/j.clay.2008.12.010

[6] Tasbihi, M., Călin, I., Šuligoj, A., Fanetti, M., Lavrenčič Štangar, U. (2017). Photocatalytic degradation of gaseous toluene by using TiO_2 nanoparticles immobilized on fiberglass cloth. *Journal of Photochemistry and Photobiology A: Chemistry*, 336, 89–97. DOI: 10.1016/j.jphotochem.2016.12.025

[7] Augugliaro, V., Bellardita, M., Loddo, V., Palmisano, G., Palmisano, L., Yurdakal, S. (2012). Review, Overview on oxidation mechanisms of organic compounds by TiO_2 in heterogeneous photocatalysis. *Journal of Photochemistry and Photobiology C: Photochemistry Reviews,* 13, 224–245. DOI: 10.1016/j.jphotochemrev.2012.04.003

[8] Tang, Y., Zhang, G., Liu, C., Luo, S., Xu, X., Chen, L., Wang, B. (2013). Magnetic TiO_2-graphene composite as a high-performance and recyclable platform for efficient photocatalytic removal of herbicides from water. *Journal of Hazardous Materials*, 252–253, 115–122. DOI: 10.1016/j.jhazmat.2013.02.053

[9] Pellegrino, F., Pellutiè, L., Sordello, F., Minero, C., Ortel, E., Hodoroaba, V.-D., Maurino, V. (2017). Influence of agglomeration and aggregation on the photocatalytic activity of TiO_2 nanoparticles. *Applied Catalysis B: Environmental*, 216, 80–87. DOI: 10.1016/j.apcatb.2017.05.046

[10] Melcher, J., Barth, N., Schilde, C., Kwade, A., Bahnemann, D. (2017). Influence of TiO_2 agglomerate and aggregate sizes on photocatalytic activity. *Journal of Materials Science*, 52(2), 1047–1056. DOI: 10.1007/s10853-016-0400-z

[11] Khalfaoui-Boutoumi, N., Boutoumi, H., Khalaf, H., David, B. (2013). Synthesis and characterization of TiO_2–Montmorillonite/ Polythiophene-SDS nanocomposites: Application in the sonophotocatalytic degradation of rhodamine 6G. *Applied Clay Science*, 80–81, 56–62. DOI: 10.1016/j.clay.2013.06.005

[12] Djellabi, R., Ghorab, M.F., Cerrato, G., Morandi, S., Gatto, S., Oldani, V., Di Michele, A., Bianchi, C.L. (2014). Photoactive TiO_2–montmorillonite composite for degradation of organic dyes in water. *Journal of Photochemistry and Photobiology A: Chemistry,* 295, 57–63. DOI: 10.1016/j.jphotochem.2014.08.017.

[13] Abdennouri, M., Baalala, M., Galadi, A., El Makhfouk, M., Bensitel, M., Nohair, K., Sadiq, M., Boussaoud, A., Barka, N. (2016). Photocatalytic degradation of pesticides by titanium dioxide and titanium pillared purified clays. *Arabian Journal of Chemistry*, 9, 313–318. DOI: 10.1016/j.arabjc.2011.04.005

[14] Djellabi, R., Ghorab, M.F., Bianchi, C.L., Cerrato, G., Morandi, S. (2016). Removal of Crystal Violet and Hexavalent Chromium using TiO_2-Bentonite under Sunlight: Effect of TiO_2 Content. *Journal of Chemical Engineering & Process Technology*, 7(1), 276. DOI: 10.4172/2157-7048.1000276

[15] Khalaf, H., Bouras, O., Perrichon, V. (1997). Synthesis and characterization of Al-pillared and cationic surfactant modified Al pillared Algerian bentonite. *Microporous Materials*, 8(3–4), 141–150. DOI: 10.1016/S0927-6513(96)00079-X

[16] Sterte, J. (1986). Synthesis and properties of titanium oxide cross linked montmorillonite. *Clays and Clay Minerals*, 34(6), 658–664. DOI: 10.1346/CCMN.1986.0340606

[17] Del Castillo, H.L., Grange, P. (1993). Preparation and catalytic activity of titanium pillared montmorillonite. *Applied Catalysis A: General*, 103, 23–34. DOI: 10.1016/0926-860X(93)85170-T.

[18] Butman, M.F., Ovchinnikov, N.L., Karasev, N.S., Kochkina, N.E., Agafonov, A.V., Vinogradov, A.V. (2018). Photocatalytic and adsorption properties of TiO_2-pillared montmorillonite obtained by hydrothermally activated intercalation of titanium polyhydroxo complexes. *Beilstein Journal of Nanotechnology*, 9, 364–378. DOI: 10.3762/bjnano.9.36

[19] Bernier, A., Admaiai, L.F., Grange, P. (1991). Synthesis and characterization of titanium pillared clays. Influence of the temperature of preparation. *Applied Catalysis,* 77, 269–281. DOI: 10.1016/0166-9834(91)80071-4.

[20] Chen, D., Du, G., Zhu, Q., Zhou, F. (2013). Synthesis and characterization of TiO_2 pillared montmorillonites: Application for methylene blue degradation. *Journal of Colloid and Interface Science*, 409, 151–157. DOI: 10.1016/j.jcis.2013.07.049.

[21] Barama, S., Dupeyrat-Batiot, C., Capron, M., Bordes-Richard, E., Bakhti-Mohammedi, O. (2009). Catalytic properties of Rh, Ni, Pd and Ce supported on Al-pillared montmorillonites in dry reforming of methane. *Catalysis Today*, 141, 385–392. DOI: 10.1016/j.cattod.2008.06.025

[22] Kruse, N., Chenakin, S. (2011). XPS characterization of Au/TiO_2 catalysts: Binding energy assessment and irradiation effects. *Applied Catalysis A: General*, 391, 367–376. DOI: 10.1016/j.apcata.2010.05.039.

[23] Boudali, L.K., Ghorbel, A., Grange, P., Figueras, F. (2005). Selective catalytic reduction of NO with ammonia over V_2O_5 supported sulfated titanium-pillared clay catalysts: influence of V_2O_5 content. *Applied Catalysis B: Environmental*, 59, 105–111. DOI: 10.1016/j.apcatb.2005.01.007

[24] Long, R.Q., Yang, R.T. (2000). Catalytic Performance and Characterization of VO^{2+} Exchanged Titania-Pillared Clays for Selective Catalytic Reduction of Nitric Oxide with Ammonia. *Journal of Catalysis*, 196(1), 73–85. DOI: 10.1006/jcat.2000.3015.

[25] Kaneko, T., Shimotsuma, H., Kajikawa, M. (2001). Synthesis and Photocatalytic Activity of Titania Pillared Clays. *Journal of Porous Materials*, 8, 295–301. DOI: 10.1023/A:1013165014982.

[26] Zhang, J., Zhang, S., Cai, W., Zhong, Q. (2013). The characterization of CrCe-doped on TiO_2-pillared clay nanocomposites for NO oxidation and the promotion effect of CeOx. *Applied Surface Science*, 268, 535–540. DOI: 10.1016/j.apsusc.2012.12.169.

[27] Liang, X., Qi, F., Liu, P., Wei, G., Su, X., Ma, L., He, H., Lin, X., Xi, Y., Zhu, J., Zhu, R. (2016). Performance of Ti-pillared montmorillonite supported Fe catalysts for toluene oxidation: The effect of Fe on catalytic activity. *Applied Clay Science*, 132–133, 96–104. DOI: 10.1016/j.clay.2016.05.022.

[28] Ding, X., An, T., Li, G., Zhang, S., Chen, J., Yuan, J., Zhao, H., Chen, H., Sheng, G., Fu, J. (2008). Preparation and characterization of hydrophobic TiO_2 pillared clay: The effect of acid hydrolysis catalyst and doped Pt amount on photocatalytic activity. *Journal of Colloid and Interface Science,* 320, 501–507. DOI: 10.1016/j.jcis.2007.12.042.

[29] Hadj Bachir, D., Khalaf, H., Ferroukhi, S., Boutoumi, Y., Schnee, J., Gaigneaux, E.M. (2020). Preparation and characterization of TiO_2 pillared clay: effect of palladium and photosensitizer on photocatalytic activity. *Research Journal of Chemistry and Environment*, 24(3), 60–73.

[30] Schoonheydt, R.A., Pinnavaia, T., Lagaly, G., Gangas, N. (1999). Pillared clays and pillared layered solids (technical report). *Pure and Applied Chemistry*, 71(12), 2367–2371. DOI: 10.1351/pac199971122367.

[31] Chen, Q., Kerk, W.T., Soutar, A.M., Zeng, X.T. (2009). Application of dye intercalated bentonite for developing latent fingerprints. *Applied Clay Science*, 44, 156–160.

[32] Sing, K.S.W., Everett, D.H. (1985). Reporting physisorption data for gas/solid systems with special reference to the determination of surface area and porosity. *Pure and Applied Chemistry*, 57(4), 603–619. DOI: 10.1351/pac198557040603

[33] Brunauer, S., Deming, L.S., Deming, W.E., Teller, E. (1940). On a Theory of the van der Waals Adsorption of Gases. *Journal of the American Chemical Society*, 62(7), 1723–1732. DOI: 10.1021/ja01864a025.

[34] Fatimah, I., Nurillahi, R., Sahroni, I., Muraza, O. (2019). TiO_2-pillared saponite and photosensitization using a ruthenium complex for photocatalytic enhancement of the photodegradation of bromophenol blue. *Applied Clay Science*, 183, 105–302. DOI: 10.1016/j.clay.2019.105302.

[35] Yamanaka, S., Makita, K. (1995). Optical and Electrochemical Properties of Titania Pillared. *Journal of Porous Materials*, 1, 29–41. DOI: 10.1007/BF00486522.

[36] Kohno, Y., Kinoshita, R., Yoda, K., Shibata, M., Matsushuma, R., Tomita, Y., Maeda, Y., Kobayashi, K. (2009). Stabilization of naturel anthocyanin by intercalation into montmorillonite. *Applied Clay Science*, 42, 519–523. DOI: 10.1016/j.clay.2008.06.012

[37] Ahmed, S., Rasul, M.G., Brown, R., Hashib, M.A. (2011). Influence of parameters on the heterogeneous photocatalytic degradation of pesticides and phenolic contaminants in wastewater: A short review. *Journal of Environmental Management*, 92, 311–330. DOI: 10.1016/j.jenvman.2010.08.028.

[38] Sutaporn, M., Thanyada, R., Nopporn, K., Somchintana, P., Varong, P. (2018). Surface-Dependence of Adsorption and Its Influence on Heterogeneous Photocatalytic Reaction: A Case of Photocatalytic Degradation of Linuron on Zinc Oxide. *Catalysis Letters*, 148, 873–881. DOI: 10.1007/s10562-018-2300-0.

[39] Ahmed, S., Rasul, M.G., Wayde, N.M., Brown, R., Hashib, M.A. (2010). Heterogeneous photocatalytic degradation of phenols in wastewater: A review on current status and developments. *Desalination,* 261, 3–18. DOI: 10.1016/j.desal.2010.04.062.

[40] Zouaghi, R., Zertal, A., David et, B., Guittonneau, S. (2007). Photocatalytic Degradation of Monolinuron and Linuron in an Aqueous Suspension of Titanium Dioxide Under Simulated Solar Irradiation. *Journal of Water Science*, 20(2), 163–172. DOI: 10.7202/015810ar.

[41] Rao, Y.F., Chu, W. (2010). Degradation of linuron by UV, ozonation, and UV/O_3 processes. Effect of anions and reaction mechanism. *Journal of Hazardous Materials*, 180, 514–523.

[42] Bahnemann, W., Muneer, M., Haque, M.M. (2007). Titanium dioxide-mediated photocatalysed degradation of few selected organic pollutants in aqueous suspensions. *Catalysis Today*, 124, 133–148. DOI: 10.1016/j.cattod.2007.03.031

[43] Mazierski, P., Nadolna, J., Lisowski, W., Winiarski, M.J., Gazda, M., Nischk, M., Klimczuk, T., Zaleska-Medynska, A. (2017). Effect of irradiation intensity and initial pollutant concentration on gas phase photocatalytic activity of TiO_2 nanotube arrays. *Catalysis Today*, 284, 19–26. DOI: 10.1016/j.cattod.2016.09.004

[44] Devi, R., Singh, V., Kumar, A. (2008). COD and BOD reduction from coffee processing wastewater using Avacado peel carbon. *Bioresource Technology,* 99(6), 1853–1860. DOI: 10.1016/j.biortech.2007.03.039.

[45] Abd El-Gawad, S.A., Abd El-Aziz, H.M. (2018). Effective removal of chemical oxygen demand and phosphates from aqueous medium using entrapped activated carbon in alginate. *MOJ Biology and Medicine*, 3(6), 227–236. DOI: 10.15406/mojbm.2018.03.00104.

[46] Das, C.P., Patnaik, L.N. (2001). Use of industrial waste for reduction of COD from paper mill effluent. *Indian Journal of Environmental Health*, 43(1), 21–27.

[47] Dyan, M.O., Putra, G.P., Budiyono, B., Sumardiono, S., Kusworo, T.D. (2015). The effect of pH and operation mode for COD removal of slaughterhouse wastewater with Anaerobic Batch Reactor (ABR). *Waste Technology*, 3(1), 7–13. DOI: 10.14710/3.1.7-13